Possible Verwey-Type Transition in $Pb_3Rh_7O_{15}$

Hiroshi Mizoguchi,[†] A. P. Ramirez,[‡] T. Siegrist,[§] L. N. Zakharov,[†] A. W. Sleight,[†] and M. A. Subramanian*,[†]

Oregon State University Materials Institute and Department of Chemistry, Oregon State University, Corvallis, Oregon 97331, LGS, 15 Vreeland Road, Florham Park, New Jersey 07932, and Department of Chemical and Biomedical Engineering, Florida State University, Tallahassee, Florida 32310

Received March 11, 2009. Revised Manuscript Received April 8, 2009

Crystals of the mixed-valence compound $Pb_3Rh_4^{3+}Rh_3^{4+}O_{15}$ have been grown in a PbO flux. These hexagonal crystals show an isotropic electrical resistivity of about 1×10^{-3} ohm cm at room temperature. This resistivity slowly increases with decreasing temperature until 185 K, where the resistivity begins increasing more rapidly as temperature is further decreased. Specific heat measurements on polycrystalline $Pb_3Rh_7O_{15}$ show a sharp, lambda-shaped peak at 185 K. Magnetic susceptibility and thermopower measurements on $Pb_3Rh_7O_{15}$ also show a discontinuity at about 185 K. Structural analyses of X-ray diffraction data obtained above and below 185 K indicate that a change in space group has occurred at 185 K. It is likely that the transition at 185 K is related to a change in charge modulation. The phase transition at 185 K fades away as Bi is substituted for Pb in $Pb_3Rh_7O_{15}$.

Introduction

Two compounds have been reported in the Pb/Rh/O system.[1−4] Synthesis of $Pb_2Rh_2O_7$ with the pyrochlore structure requires high pressure.[1] The compound $Pb_3Rh_7O_{15}$ can, however, be prepared by heating a mixture of PbO and Rh_2O_3 in air.[2−4] The structure of $Pb_3Rh_7O_{15}$ was reported 30 years ago,[3,4] and a phase transition at 185 K was also reported.[3] However, the details of this phase transition have never been reported until now. This delay has been caused primarily by the difficulty in understanding this transition and the structure below the transition. We believe that publishing the details of this transition should not be further delayed despite our incomplete understanding.

Experimental Section

Reactants were Bi_2O_3 (99.9% Baker), PbO (99.9% Aldrich), and Rh_2O_3 prepared from $RhCl_3 \cdot xH_2O$(99.9%, Alfa Aesar) by heating in moist air at 1073 K for 10 h. Appropriate amounts of these oxides were mixed by grinding together under ethanol in an agate mortar and pestle. This pressed mixture was placed in an alumina boat and heated in air at 973 K for 10 h, and then at 1073 K for 10 h with intermediate grinding. X-ray powder diffraction patterns were obtained with a RIGAKU MINIFLEX II using Cu Kα radiation and a graphite monochromator. Single crystals of $Pb_3Rh_7O_{15}$ were grown in a PbO flux. An intimate mixture of PbO (12.6 g, 56.5 mmol) and Rh_2O_3 (0.63 g, 2.5 mmol) was thoroughly mixed and heated to 1373 K in air in a platinum crucible. After holding for 10 h, the crucible was cooled to 1223 K at a rate of 3 K/h. After reaching 1223 K, it was cooled to room temperature at a rate of 200 K/h. The flux was dissolved in HNO_3 (aq.) at 363 K. The black crystals were platelike with dimensions up to 0.5 × 2 mm.

Single-crystal X-ray diffraction data were collected at 293 and 110K using a Bruker SMART APEXII CCD system and an Oxford Cryostream Cooler. A fine focus tube was used with an anode power of 50 KV at 30 mA, a crystal to plate distance of 6.0 cm, 512 × 512 pixels/frame, beam center (256.52, 253.16), φ/ω scan with step of 0.30°, exposure/frame of 10.0 s/frame, and SAINT integration. An absorption correction was applied by SADABS. The crystal structure was solved by direct methods and refined with full-matrix least-squares method using the SHELXTL package. Further measurements to higher angles were carried out using an Oxford-Diffraction Xcalibur2 CCD diffractometer, equipped with a Cryojet cooling device. DC electrical conductivities measurements were conducted by the conventional four-probe method over the temperature region 5−300 K. Seebeck coefficient measurements were conducted over the temperature region 5−300 K using static method by maintaining a fixed temperature difference between both ends of the samples and voltage developed was measured using a precision nanovoltmeter. Magnetic susceptibility data were obtained with a Quantum Design MPMS SQUID magnetometer. Specific heat data were obtained using a conventional thermal relaxation technique (semiadiabatic heat-pulse method) using Quantum Design PPMS.

Results

Electrical resistivity measurements on several $Pb_3Rh_7O_{15}$ single crystals showed a room temperature resistivity of about 1×10^{-3} ohm-cm, which initially increases only slowly with decreasing temperature. However, below 185 K there is an abrupt increase in slope similar to that associated with charge ordering (Figure 1a). Measurements perpendicular and parallel to the *c* axis give the same values within the 10% error

* Corresponding author. E-mail: mas.subramanian@oregonstate.edu.
[†] Oregon State University.
[‡] LGS.
[§] Florida State University.

(1) Sleight, A. W. *Mater. Res. Bull.* **1971**, *6*, 775.
(2) Boonstra, A. H.; Mutsaers, C. A. H. A. *Thin Solid Films* **1978**, *51*, 287.
(3) Sleight, A. W.; Chen, H.-Y.; Gillson, J. L. *ACS/CSJ Chemical Congress*, Honolulu, HI, April 1−6, 1979; American Chemical Society: Washington, D.C., 1979; p 75.
(4) Omaly, P. J.; Kohlmuller, R.; Batail, P.; Chevalier, R. *Acta Crystallogr., Sect. B* **1980**, *36*, 1040.
(5) Sheldrick, G. M., *SHELXTL, version 6.14*; Bruker Analytical X-ray Instruments, Inc.: Madison, WI, 2003.

10.1021/cm900697s CCC: $40.75
Published on Web 04/27/2009

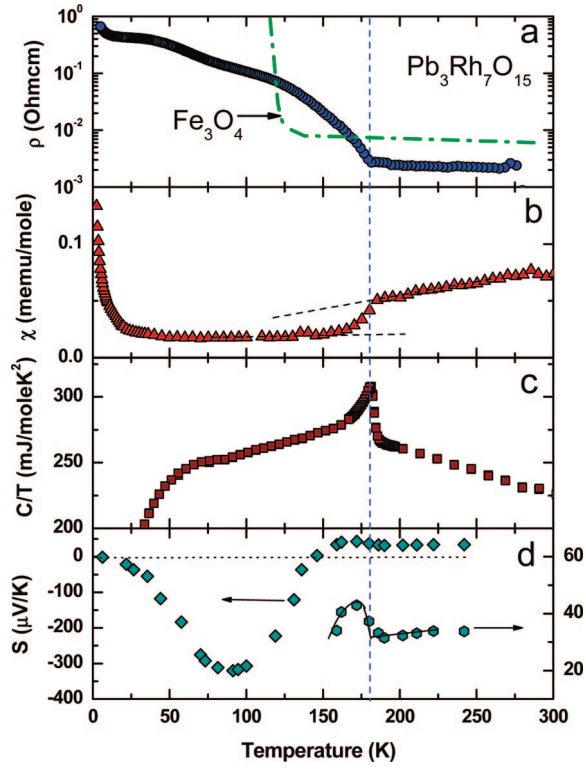

Figure 1. Properties vs temperature for $Pb_3Rh_7O_{15}$: (a) electrical resistivity, with points including data both perpendicular and parallel to the *c* axis; (b) magnetic susceptibility; (c) heat capacity; and (d) Seebeck coefficient. The octagon points (corresponding to right-hand-side *y*-axis) show the enlarged Seebeck data near the transition.

in measuring the distance between probes. Magnetic susceptibility measurements on a single crystal of $Pb_3Rh_7O_{15}$ also show a discontinuous drop at 185 K (Figure 1b). At 185 K, specific heat measurements on polycrystalline $Pb_3Rh_7O_{15}$ show a sharp peak with a lambda shape indicative of a second order transition with an entropy of ~0.8 J/((mol Rh) K) (Figure 1c). The Seebeck coefficient measured on a sintered pellet changes from positive to negative with decreasing temperature and shows a small but distinct discontinuity at 185 K (Figure 1d).

The room-temperature structure of $Pb_3Rh_7O_{15}$ based on space group $P6_3/mcm$ was refined using single-crystal X-ray diffraction data. Results are summarized in Tables 1−3 and the available cif file in the Supporting Information. The result is essentially the same as previously reported,[3,4] and the structure is shown in Figure 2. The Pb atoms in the hexagonal cages are strongly displaced to the sides of the cages, such that all Pb−O bonds are on one side of the Pb atoms. The only compound known to be isostructural with $Pb_3Rh_7O_{15}$ is $Pb_3Mn_7O_{15}$, which has been refined in the space groups $Cmc2_1$, $Cmcm$, and $P6_3/mcm$.[6] Low-temperature powder X-ray diffraction indicated that the cell edges varied smoothly through the transition at 185 K. Single-crystal X-ray diffraction patterns obtained at 110 K suggested no change in space group. However, attempts to refine this structure in space group $P6_3/mcm$ using intensity data collected at 110 K always led to physically meaningless displacement factors for several atoms. Furthermore, on going from the 293 K to the 110 K data, the *R* value of 0.017 increased to 0.043 and the largest peak/hole in the difference maps increased from 1.55/−0.99 to 4.0/−3.75 e/Å^3. This indicates that the space group has actually changed on going through the transition at 185 K. Attempts were made to refine the structure in other hexagonal and trigonal space groups including $P6_3cm$, $P\bar{6}c2$, $P3c1$, $P\bar{3}1m$, and $P3$. None of these attempts produced a result with reasonable displacement factors. Likewise, attempts to obtain a well-behaved refinement assuming a twinned orthorhombic structure in space groups such as $Cmc2_1$, $Cmcm$, and $C222_1$ failed. Merohedral twinning based on trigonal symmetry (retaining a hexagonal metric) is a possibility. To address such twinning, we collected high-resolution powder diffraction data for $Pb_3Rh_7O_{15}$ at the NSLS synchrotron at 80 K and room temperature. These data showed no evidence of a metric distortion from hexagonal symmetry. Various structural refinements of these data in subgroups of $P6_3/mcm$ have yielded no results with reasonable displacement factors, regardless of the space group

Table 1. Crystallographic Information for $Pb_3Rh_7O_{15}$ and $Pb_{1.8}Bi_{1.2}Rh_7O_{15}$

empirical formula	$Pb_3Rh_7O_{15}$	$Pb_{1.8}Bi_{1.2}Rh_7O_{15}$
fw	1581.94	1583.66
T (K)	293 (2)	268(2)
wavelength (Å)	0.71073	0.71073
cryst syst	hexagonal	hexagonal
space group	$P6_3/mcm$	$P6_3/mcm$
a (Å)	10.3537(2)	10.351(5)
c (Å)	13.2837(5)	13.152(13)
V (Å^3)	1233.22(6)	1220.3(14)
Z	4	4
D (calculated) (g cm^{-3})	8.520	8.620
absorp coeff (mm^{-1})	49.989	51.116
F(000)	2724	2728
cryst size (mm^3)	0.06 × 0.04 × 0.03	0.03 × 0.02 × 0.01
θ range (deg)	2.27−26.99	2.27−27.49
index ranges	$-8 \le h \le 13$ $-13 \le k \le 12$ $-16 \le l \le 16$	$-13 \le h \le 11$ $-12 \le k \le 13$ $-16 \le l \le 17$
reflns collected	8041	9490
independent reflns	522 [R_{int} = 0.0374]	544 [R_{int} = 0.0458]
completeness to θ = 26.99° (%)	100.0	100.0
max. and min transmission	0.3155 and 0.1534	0.6289 and 0.3093
refinement method	full matrix least-squares on F^2	full matrix least-squares on F^2
data/restraints/params	522/0/51	544/0/51
GOF on F^2	1.209	1.276
final *R* indices [$I > 2\sigma(I)$]	R_1 = 0.0170, wR_2 = 0.0391	R_1 = 0.0212, wR_2 = 0.0487
R indices (all data)	R_1 = 0.0173, wR_2 = 0.0392	R_1 = 0.0228, wR_2 = 0.0504
extinction coeff	0.00251(7)	0.00015(2)
largest diff. peak and hole	1.55 and −0.99 e Å^{-3}	1.497 and −1.587 e Å^{-3}

Table 2. Atomic Coordinates and Equivalent Isotropic Displacement Parameters for $Pb_3Rh_7O_{15}$ at 293 K

	Wyckoff	*x*	*y*	*z*	U_{eq}[a]
Pb1	6g	0	0.3951(1)	1/4	11(1)
Pb2	6g	0.7365(1)	0	1/4	9(1)
Rh1	8h	2/3	1/3	0.1487(1)	4(1)
Rh2	12i	0.6634(1)	−0.1683(1)	0	4(1)
Rh3	2b	0	0	0	5(1)
Rh4	6f	1/2	0	0	4(1)
O1	12k	0.6664(5)	0	0.0792(4)	5(1)
O2	12k	0.8309(5)	−0.1691(5)	0.0768(4)	7(1)
O3	24l	0.8418(4)	0.3346(4)	0.818(3)	7(1)
O4	12j	0.5199(6)	0.3423(6)	1/4	4(1)

[a] U_{eq} (Å^2 × 10^3) is defined as one-third of the trace of the orthogonalized U^{ij} tensor.

(6) Le Page, Y.; Calvert, L. D. *Acta Crystallogr., Sect. C* **1984**, *40*, 1787.

Table 3. Selected Interatomic Distances (Å) for $Pb_3Rh_7O_{15}$ at 293 K and $Pb_{1.8}Bi_{1.2}Rh_7O_{15}$ at 268 K

	$Pb_3Rh_7O_{15}$	$Pb_{1.8}Bi_{1.2}Rh_7O_{15}$
Rh1−O3	2.014(4) × 3	2.007(5) × 3
Rh1−O4	2.067(4) × 3	2.082(5) × 3
Rh2−O3	1.993(4) × 2	2.000(5) × 2
Rh2−O2	2.016(4) × 2	2.017(4) × 2
Rh2−O1	2.022(4) × 2	2.029(5) × 2
Rh3−O2	2.026(5) × 6	2.030(7) × 6
Rh4−O3	1.998(4) × 4	2.002(5) × 4
Rh4−O1	2.019(6) × 2	2.009(7) × 2
Pb1/Bi1−O4	2.403(5) × 2	2.367(7) × 2
Pb1/Bi1−O3	2.654(4) × 4	2.605(5) × 4
Pb2/Bi2−O4	2.355(6) × 2	2.333(7) × 2
Pb2/Bi2−O1	2.382(5) × 2	2.361(7) × 2

assumed. None of the low- temperature X-ray diffraction data showed any superstructure. Likewise, electron diffraction studies in an electron microscope showed no evidence of superstructure reflections below 185 K. Thus, although a lowering of the symmetry occurs at 185 K, displacements of atoms breaking the symmetry are apparently small.

Substitution of Bi according to $Pb_{3-x}Bi_xRh_7O_{15}$ was successful up to about $x = 1.2$, causing the unit-cell edges to change from $a = 10.360$ and $c = 13.30$ Å to $a = 10.364$ and $c = 13.19$ Å. This change seems reasonable because Bi^{3+} is much smaller than Pb^{2+}, but for every atom of Bi substituted, one Rh^{4+} cation is converted to a larger Rh^{3+} cation. The transition at 185 K fades away as Bi is substituted for Pb (Figure 3). Single crystals of a $Pb_{3-x}Bi_xRh_7O_{15}$ composition were grown from a Bi_2O_3/V_2O_5 flux. Results of a single crystal X-ray diffraction analyses for data obtained at 268 K are given in Tables 1, 3, and 4 as well as the available cif file in the Supporting Information. The composition of the crystal used was determined from microprobe data to be $Pb_{2.04}Bi_{0.96}Rh_7O_{15}$. Single crystal X-ray diffraction data were also collected on this crystal at 120 and 173 K. These data refined in space group $P6_3/mcm$ showed no significant change in R values relative to that obtained at 268 K. However, the displacement factor for one oxygen atom became negative, and systematic discrepancies were noted for $00l$ reflections. This suggests a deviation from space group $P6_3/mcm$ has occurred but that the change in structure below 185 K is much less than for $Pb_3Rh_7O_{15}$.

Discussion

Before discussing the transition in $Pb_3Rh_7O_{15}$, we need to consider just how well we understand this compound at room temperature. Given the mixed valency in $Pb_3Rh_7O_{15}$, one can consider the possibility of charge ordering on the four different Rh sites (Figure 2). In a review of rhodium oxides, Müller-Buschbaum considered possible Rh^{3+}/Rh^{4+} ordering schemes in $Pb_3Rh_7O_{15}$ based on lattice energy calculations, concluding that the favored ordering scheme depended on how the lone pair of Pb^{2+} was treated.[7] We have approached the question of charge ordering from the point of view of bond valence sums. In the room-temperature structure of $Pb_3Rh_7O_{15}$, there are four different crystallographic sites for Rh (Figure 2). For a $Pb_3Rh_4^{3+}Rh_3^{4+}O_{15}$ formulation, a simple way to charge order on the given crystallographic sites would be to place Rh^{4+} on the 12i sites (gray octahedra in Figure 2b) and Rh^{3+} on all the other sites. However, this is not consistent with the bond valence sums in Table 5 because this site does not have the highest bond valence sum. The oxygen layers sandwiching the Rh layers shown in Figure 2b are hexagonally close packed. Rh atoms fill 5/6 of the octahedral sites between the oxygen layers. The arrangement of the vacant octahedral sites leads to 3 distinct Rh sites in this layer. Possible charge modulation could be viewed as a relative occupation of $Rh^{3+}$and Rh^{4+} on the various sites, and simple electrostatics would dictate that Rh^{4+}would be found in octahedra sharing the fewest edges, in order to decrease the Rh−Rh repulsion term across shared edges. Given the high electrical conductivity, one can view any charge modulation on the Rh lattice as the relative occupation of holes in the 4d t_{2g} band without reference to oxidation states. A Rh^{3+} rhodate would have a filled t_{2g} band, and a Rh^{4+} rhodate would have one hole/Rh in this band. In the Rh−O layers of $Pb_3Rh_7O_{15}$, one could then expect that the hole concentration will be at a minimum for the sites with the maximum number of shared edges. This logic leads to the conclusion of a minimum hole concentration for the octahedra sharing 6 edges (dark blue octahedral in Figure 2b) and the maximum concentration of holes for octahedra sharing 4 edges (green octahedra in Figure 2b). An intermediate concentration of holes would occur for the octahedra sharing 5 edges (gray octahedra in figure 2b). This model is supported by bond valence calculations for these 3 Rh atoms, which give values of 3.26, 3.89, and 3.45, respectively (Table 5). A very low concentration of holes is expected for Rh atoms in the octahedra sharing faces (light blue octahedral in Figure 2a), and again, this is supported by the valence sum of 3.14. If it were not for the high electrical conductivity, we might then assume that Rh^{3+}occupies the light and dark blue octahedra, that Rh^{4+} occupies the green octahedra, and that the gray octahedra are occupied by equal amounts of Rh^{3+} and Rh^{4+}. The formulation is then $Pb_6Rh_5^{3+}Rh_6^{3.5+}Rh_3^{4+}O_{30}$. In a $Pb_3Rh_4^{3+}Rh_3^{4+}O_{15}$ formulation, there is no possible structure for $Pb_3Rh_7O_{15}$ where all Rh near neighbors of Rh^{3+} would be Rh^{4+} and all Rh near neighbors of Rh^{4+} would be Rh^{3+}. The $Pb_6Rh_5^{3+}Rh_6^{3.5+}Rh_3^{4+}O_{30}$ formulation is a good compromise because in the sheets (Figure 2b) Rh^{3+} and Rh^{4+} are separated by $Rh^{3.5+}$. Such a formulation is in reasonable agreement with the bond valence sums in Table 5. Bond valence sums in mixed valent compounds never reach the values expected from the oxidation states.[8] For example, in insulating $Ca_2Fe^{3+}Fe^{5+}O_6$, the bond valence sums for Fe^{3+} and Fe^{5+} are 3.48 and 4.58, respectively, and in $NdBaFe^{2+}Fe^{3+}O_5$, the bond valence sums are 2.20 and 2.87, respectively.[9,10] This deviation is caused by a mixing of the Fe^{3+} and Fe^{5+} states as a consequence of the strong overlap the 3d orbitals of these two cations with the

(7) Müller-Buschbaum, H. *Z. Anorg. Allg. Chem.* **2007**, *633*, 1289.
(8) Attfield, J. P. *Solid State Sci.* **2006**, *8*, 861.
(9) Woodward, P. M.; Cox, D. E.; Moshopoulou, E.; Sleight, A. W.; Morimoto, S. *Phys. Rev. B* **2000**, *62*, 844.
(10) Woodward, P. M.; Suard, E.; Karen, P. *J. Am. Chem. Soc.* **2003**, *125*, 8889.

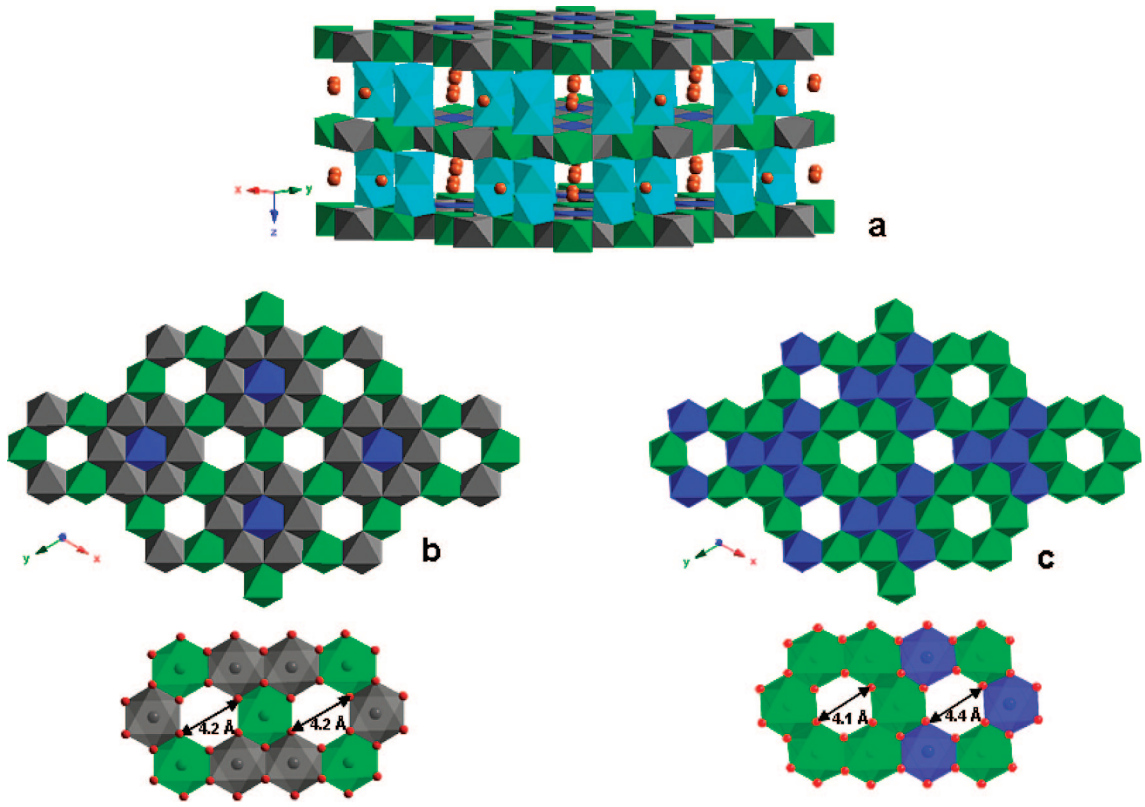

Figure 2. (a) $Pb_3Rh_7O_{15}$ structure shown as RhO_6 octahedra and yellow spheres for Pb. (b) Charge modulation of the RhO_6 octahedra where the highest charge (green) is separated from the lowest charge (blue) by octahedra of intermediate charge (gray). (c) A possible new modulation that occurs below 185 K.

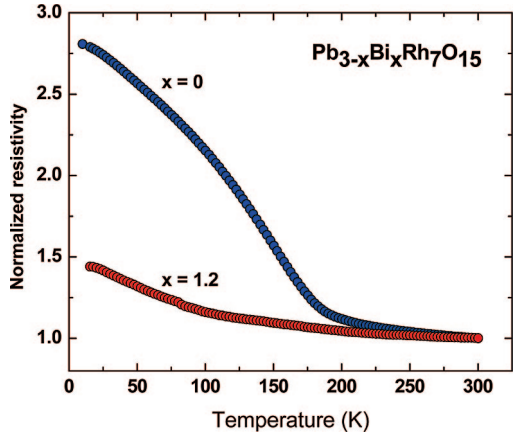

Figure 3. Normalized electrical resistivity (ρ_T/ρ_{298K}) vs temperature for $Pb_{3-x}Bi_xRh_7O_{15}$ (sintered polycrystalline samples).

bonding orbitals of the same oxygen atoms. Covalency of a cation−anion bond reduces the real charge on the cation and anion, but the oxidation states are not impacted and this covalency has little impact on bond distances and bond valence sums. The impact of covalency is very different for the mixed valent cations. The covalency in a Fe^{3+}−O−Fe^{5+} linkage will result in some transfer of electron density from Fe^{3+} to Fe^{5+}, which will then have the expected impact on Fe−O distances and give a high bond valence sum for Fe^{3+} and a low bond valence sum for Fe^{5+}. Thus, in a Rh^{3+}/Rh^{4+} mixed-valence oxide, bond valence sums of 3.26 and 3.89 (Table 5) are consistent with Rh^{3+} and Rh^{4+} species, respectively. However, given the high electrical conductivity in $Pb_3Rh_7O_{15}$ at room temperature, it is more appropriate to describe the situation as

Table 4. Atomic Coordinates and Equivalent Isotropic Displacement for $Pb_{1.8}Bi_{1.2}Rh_7O_{15}$ at 268 K

	x	*y*	*z*	U_{eq}[a]
Pb1/Bi1	0	0.3965(1)	1/4	16(1)
Pb2/Bi2	0.7361(1)	0	1/4	12(1)
Rh1	2/3	1/3	0.1482(1)	4(1)
Rh2	0.6641(1)	−0.1680(1)	0	5(1)
Rh3	0	0	0	4(1)
Rh4	1/2	0	0	5(1)
O1	0.6660(6)	0	0.0791(5)	6(1)
O2	0.1680(6)	0	0.0796(5)	8(1)
O3	0.4914(5)	0.1570(5)	0.0838(4)	6(1)
O4	0.8260(8)	0.4815(8)	1/4	5(1)

[a] U_{eq} ($Å^2 \times 10^3$) is defined as one-third of the trace of the orthogonalized U^{ij} tensor.

Table 5. Summary of Bond Distances and Bond Valence Sums[a] for $Pb_3Rh_7O_{15}$

atom	average distance (Å) (bond valence sum)	color in figure 2
Rh1	2.041 (3.14)	light blue
Rh2	2.010 (3.45)	grey
Rh3	2.026 (3.26)	dark blue
Rh4	2.005 (3.89)	green
Pb1	2.57 (1.83)	orange
Pb2	2.37 (2.00)	orange

[a] Bond valence sums were determined using the Rh−O and Pb−O distances in Table 3.

modulation of electron density similar to that which can occur in a charge density wave.

Charge ordering in mixed-valence rhodates is not common, but it has been reported for $(Bi_6O_5)Rh_{12}O_{24}$ and $R_{18}Li_8Rh_5O_{39}$

(11) Mizoguchi, H.; Marshall, W. J.; Ramirez, A. P.; Sleight, A. W.; Subramanian, M. A. *J. Solid State Chem.* **2007**, *180*, 3463.

compounds where R can be La or Pr.[11,12] For $(Bi_6O_5)Rh_{12}O_{24}$, the charge ordering is not complete, just as it is not complete for $Pb_3Rh_7O_{15}$ or Fe_3O_4 at room temperature. In $(Bi_6O_5)Rh_4^{3+}Rh_8^{3.5+}O_{24}$, some Rh sites contain Rh^{3+} only, whereas others contain a disordered mixture of $Rh^{3+}$and Rh^{4+}. The analogous situation for Fe_3O_4 at room temperature is $Fe^{3+}Fe_2^{2.5+}O_4$ with ordering of Fe^{3+} to the tetrahedral sites but no charge ordering of Fe^{3+} and Fe^{2+} on the octahedral sites. A difficulty in determining charge ordering in rhodates is the small size difference between $Rh^{3+}$and Rh^{4+}, ~0.06 Å,[13] limiting the expected lattice strain because of charge ordering. For comparison, the difference in ionic radii for Fe^{2+} and Fe^{3+} in high spin states is twice this, 0.135 Å.[13] Also, good valence bond parameters needed to be determined for $Rh^{3+}$and Rh^{4+} (see the Supporting Information).

A phase transition in $Pb_3Rh_7O_{15}$ at 185 K is indicated by electrical resistivity, magnetic susceptibility, Seebeck coefficient, and specific heat data. The observed properties are intermediate between those expected of a classical metal or semiconductor both above and below the transition. Such intermediate behavior is common for Rh^{4+} rhodates and for mixed valent Rh^{3+}/Rh^{4+} rhodates,[14−18] although none of these previously studied rhodates shows the abrupt changes as seen in $Pb_3Rh_7O_{15}$. The behavior of $Pb_3Rh_7O_{15}$ is, however, reminiscent of the Verwey transition in Fe_3O_4. Although the Verwey transition in Fe_3O_4 at 119 K (Figure 1a) is frequently referred to as a metal-semiconductor transition, $d\rho/dT < 0$ at all temperatures, as is the case for $Pb_3Rh_7O_{15}$. The underlying cause of the transition in $Pb_3Rh_7O_{15}$ is likely similar to that of Fe_3O_4. In the case of Fe_3O_4 at room temperature, Fe^{3+} occupies the tetrahedral sites of the spinel structure and the average oxidation state on octahedral sites is +2.5 with no charge ordering between Fe^{2+} and Fe^{3+}. This then is analogous to $Pb_3Rh_7O_{15}$ where there is mixed valency on one site but not others. For Fe_3O_4 below 119 K, charge ordering of Fe^{2+} and Fe^{3+} on the octahedral sites is presumed to have occurred. However, this charge ordering is geometrically frustrated, and the actual structure of the charge ordered state has never been completely determined despite enormous effort.[19,20] There are, however, many mixed-valence oxides where two cations of different oxidation states in equal amounts comprise a simple cubic lattice. There is no frustration for ordering these to a face-centered cubic lattice as occurs in the perovkites $Ca_2Fe^{3+}Fe^{5+}O_6$ and $Ba_2Bi^{3+}Bi^{5+}O_6$.[9,21] In these charge-ordered structures, all near neighbors of 3+ cations are 5+ cations and all near neighbors of 5+ cations are 3+ cations. Mixed valent compounds of the formula $R^{3+}A^{2+}M^{2+}M^{3+}O_{6-x}$ with M = Fe, Mn, or Co have a slab of the same cubic lattice for the M cations, but these cation frequently charge order into structures where some near neighbors have the same oxidation state.[10,22,23] Thus, charge-ordered structures are well-known with some cations having the same oxidation state cations as near neighbors, even when this could be avoided.

Assuming that the modulation shown in Figure 2b is occurring above 185 K and is approximated as $Pb_6Rh_5^{3+}Rh_6^{3.5+}Rh_3^{4+}O_{30}$, one might expect that the new structure below 185 K separates $Rh^{3.5+}$ cations into Rh^{3+} and Rh^{4+} cations, even though such a process necessarily produces a structure with Rh near neighbors in the same oxidation state. Such an ordering scheme is shown in Figure 2c, and space group $P\bar{6}c2$ allows for such ordering. Refinement in $P\bar{6}c2$ results in a drop of *R* to 0.0409 relative to the *R* of 0.0433 that results from refinement in $P6_3/mcm$. This refinement in $P\bar{6}c2$ gives bond valence sums of 3.36 and 3.85 for the two Rh atoms that were equivalent in $P6_3/mcm$ with the single bond valence sum of 3.45 at room temperature. There are now two different sizes for the empty hexagonal rings (Figure 2c) with the smaller ring surrounded by the Rh with the higher bond valence and smaller size. However, this refinement results in negative displacement factors for several atoms. Thus, the true space group is undetermined and presumably is of lower symmetry than $P\bar{6}c2$.The modulation shown in Figure 2c is then only a suggestion of a possible additional modulation that may occur below 185 K.

A Verwey-type transition can be defined as a charge-ordering transition resulting in a significant increase in electrical resistivity below the transition. Some reported examples of this type of transition in oxides containing the 3d transition metal cations are Ti_4O_7, $R^{3+}NiO_3$ perovkites, and compounds of the type $R^{3+}A^{2+}M_2O_{6-x}$, where M can be Fe, Mn, or Co.[10,22–26] Verwey-type transitions are also reported for the mixed-valent rare earth arsenides Eu_4As_3 and Yb_4As_3.[27,28]

There are transitions in oxides containing 4d and 5d cations where the electrical resistivity rises rapidly below the transition, but they appear unrelated to charge ordering. Contrasting the transition in $Pb_3Rh_7O_{15}$ with that which occurs in $Cd_2Os_2O_7$ at 225 K shows both similarities and differences.[29] In both cases, the electrical resistivity above the transitions is between 1×10^{-3} and 1×10^{-4} ohm cm. The temperature dependence of the electrical resistivity above

(12) Frampton, P. P. C.; Battle, P. D.; Ritter, C. *Inorg. Chem.* **2005**, *44*, 7138.
(13) Shannon, R. D. *Acta Crystallogr., Sect. B* **1970**, *26*, 447.
(14) Yamaura, K.; Huang, Q.; Young, D. P.; Takayama-Muromachi, E. *Chem. Mater.* **2004**, *16*, 3424.
(15) Shimura, T.; Itoh, M.; Inaguma, Y.; Nakamura, T. *Phys. Rev. B* **1994**, *49*, 5591.
(16) Mizoguchi, H.; Ramirez, A. P.; Zakharov, L. N.; Sleight, A. W.; Subramanian, M. A. *J. Solid State Chem.* **2008**, *181*, 56.
(17) Mizoguchi, H.; Zakharov, L. N.; Ramirez, A. P.; Marshall, W. J.; Sleight, A. W.; Subramanian, M. A. *Inorg. Chem.* **2009**, *48*, 204.
(18) Mizoguchi, H.; Zakharov, L. N.; Marshall, W. J.; Sleight, A. W.; Subramanian, M. A. *Chem. Mater.* **2009**, *21*, 994.
(19) Wright, J. P.; Attfield, J. P.; Radelli, P. G. *Phys. Rev. B* **2002**, *66*, 214422.
(20) Walz, F. *J. Phys.: Condens. Matter* **2002**, *14*, R285.
(21) Cox, D. E.; Sleight, A. W. *Acta Crystallogr., Sect. B* **1979**, *35*, 1.
(22) Rao, C. N. R.; Arulraj, A.; Cheetham, A. K.; Raveau, B. *J. Phys.: Condens. Matter.* **2000**, *12*, R83.
(23) Vogt, T.; Woodward, P. M.; Karen, P.; Hunter; Henning, B. A. P.; Moodenbaugh, A. R. *Phys. Rev. Lett.* **2000**, *13*, 2969.
(24) Mott, N. F. *Philos. Mag., B* **1980**, *42*, 327.
(25) Lacorre, P. J. B.; Torrance, J. B.; Pannetier, J. S. A. I.; Nazzal, A.I. P. W.; Wang, P. W. T. C.; Huang, T. C. *J. Solid State Chem.* **1991**, *91*, 225.
(26) Alonso, J. A.; Martínez-Lope, M. J.; Casais, M. T.; García-Muñoz, J. L.; Fernández-Díaz, M. T. *Phys. Rev. B* **2000**, *61*, 1756.
(27) Wortmann, G.; Sampathkumaran, E. V.; Kaindl, G. *J. Magn. Magn. Mater.* **1986**, *54−57*, 338.
(28) Aoki, H.; Ochiai, A.; Suzuki, T.; Helfrich, R.; Steglich, F. *Physica B* **1997**, *230−232*, 698.
(29) Sleight, A. W.; Gillson, J. L.; Weiher, J. F.; Bindloss, W. *Solid State Commun.* **1974**, *14*, 357. and unpublished results. .

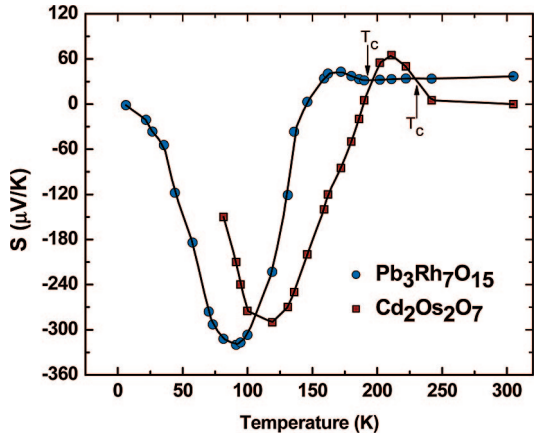

Figure 4. Seebeck coefficients vs temperature for $Cd_2Os_2O_7$ and $Pb_3Rh_7O_{15}$. Data for $Cd_2Os_2O_7$ are from ref 29.

the transitions is very weak in both cases, but with opposite slopes. Heat capacity measurements show a lambda-shaped peak in both cases indicating a second-order transition. The temperature dependence of the Seebeck coefficient is very similar for the two compounds (Figure 4). The magnetic susceptibility for both compounds is intermediate between Pauli and Curie−Weiss behavior. The pyrochlore structure of $Cd_2Os_2O_7$ has a frustrated lattice, but there is a sharp peak in the magnetic susceptibility at 225 K suggestive of magnetic order. Neutron diffraction, however, has shown no indication of magnetic order below the transition.[30] A decrease in magnetic susceptibility below the transition occurs for both $Cd_2Os_2O_7$ and $Pb_3Rh_7O_{15}$. Despite some similarities in these two transitions, $Cd_2Os_2O_7$ has no mixed valency and its metal-semiconductor transition is likely related to its half-filled 5d t_{2g} band.[29,31] A transition similar to that which occurs in $Cd_2Os_2O_7$ also occurs in $Hg_2Ru_2O_7$ but not in $Cd_2Ru_2O_7$ or $Hg_2Os_2O_7$.[32−34] Another pyrochlore with a metal−insulator transition is $Tl_2Ru_2O_7$,[35] but that transition is abrupt, first-order, and shows considerable hysteresis, unlike the transitions in $Cd_2Os_2O_7$ and $Pb_3Rh_7O_{15}$. The oxidation state situation in $Tl_2Ru_2O_7$ is very complex because of the strong contribution of both Ru 4d and Tl 6s states at the Fermi level. Structural studies have suggested that a charge ordering transition may occur in $Ba_3NaRu_2O_9$ at 225 K.[36] However, subsequent electrical resistivity measurements show no increase resistivity at or just below 225 K.[37] It thus appears that $Pb_3Rh_7O_{15}$ is the only known candidate for a classical Verwey-type transition in an oxide where the cation is not a 3d cation.

We conclude that the charge modulation in $Pb_3Rh_7O_{15}$ above 185 K changes below 185 K but we were unable to determine the precise structure below 185 K. This failure is perhaps not surprising considering that the many attempts to precisely define the charge modulation in Fe_3O_4 below 119 K have failed. Although the Pb coordination and valence bond sums (Table 5) in $Pb_3Rh_7O_{15}$ indicate that Pb is Pb^{2+}, the Pb 6p band is not far above the Fermi level and significant mixing of Pb 6p states into the Rh 4d t_{2g} band can be expected. This may then have an impact on the electron delocalization, especially along the *c* axis. The mixing of Pb 6p states into the Rh 4d t_{2g} band may also impact any charge modulation on the Rh lattice.

Acknowledgment. We thank P. Stevens, NSLS, for support in the powder diffraction data acquisition at beamline X16C and Dr. Maryvonne Hervieu, CRISMAT Laboratory for electron diffraction results. The work at Oregon State University is supported by grants from the National Science Foundation (DMR 0804167) and Air Force Research Laboratory (FA8650-05-1-5041).

Supporting Information Available: Crystallographic information in CIF format; additional information on the bond valence parameters (PDF). This information is available free of charge via the Internet at http://pubs.acs.org.

CM900697S

(30) Reading, J.; Weller, M. T. *J. Mater. Chem.* **2001**, *11*, 2373.
(31) Mandrus, D.; Thompson, J. R.; Gaal, R.; Forro, L.; Bryan, J. C.; Chakoumakos, B. C.; Woods, L M.; Sales, B. C.; Fishman, R. S.; Keppens, V. *Phys. Rev. B* **2001**, *63*, 195104.
(32) Klein, W.; Kremer, R. K.; Jansen, M. *J. Mater. Chem.* **2007**, *17*, 1356.
(33) Reading, J.; Gordeev, S.; Weller, M. I. *J. Mater. Chem.* **2002**, *12*, 646.
(34) Wang, R.; Sleight, A. W. *Mater. Res. Bull.* **1998**, *33*, 1005.
(35) Jarrett, H. S.; Sleight, A. W.; Weiher, J. F.; Gillson, J. L.; Frederick, C. G.; Jones, G. A.; Swingle, R. S.; Swartzfager, D.; Gulley, J. E.; Hoell, P. C. *Valence Instabilities and Related Narrow-Band Phenomena*; Plenum: New York, 1977; pp 545−549.
(36) Stitzer, K. E.; Smith, M. D.; Gemmill, W. R.; zur Loye, H. C. *J. Am. Chem. Soc.* **2002**, *124*, 13877.
(37) Samata, H.; Kai, M.; Uchida, T.; Ohtsuka, M.; Tanaka, G.; Sawada, S.; Taniguchi, T.; Nagata, Y. *J. Alloys Compd.* **2003**, *350*, 77.